



# Predicting conditional maximum contaminant level exceedance probabilities for drinking water after wildfires with Bayesian regularized network ensembles



Andres Schmidt <sup>a,\*</sup>, Lisa M. Ellsworth <sup>a</sup>, Jenna H. Tilt <sup>b</sup>, Mike Gough <sup>c</sup>

<sup>a</sup> Department of Fisheries, Wildlife and Conservation Sciences, Oregon State University, Corvallis, OR, USA

<sup>b</sup> Department of Geography, Environmental Sciences, and Marine Resource Management, Oregon State University, Corvallis, OR, USA

<sup>c</sup> Conservation Biology Institute, Corvallis, OR, USA

## ARTICLE INFO

### Keywords:

Bayesian-regularized network ensembles  
Conditional probabilities of drinking water contamination  
Post-wildfire risk to water distribution systems (WDS) in the wildland urban interface (WUI)  
Maximum contaminant level (MCL) exceedance probabilities

## ABSTRACT

The severity and frequency of wildfires have increased throughout the Pacific Northwest in recent decades, costing lives and destroying large amounts of valuable resources and assets. This trend is predicted to persist because of climate change and the associated increased fire risk caused by prolonged droughts in combination with changes in land cover and land use, including rapid increases in wildland urban interface areas. The threat of benzene and other contaminants in drinking water from water distribution systems after wildfires is a relatively recently discovered problem that gained attention because of the significant health hazards that high levels of benzene in drinking water pose for humans. Driving processes leading to post-fire benzene contamination in water distribution systems are largely unknown. Currently, no deterministic process models exist to predict the risk of exceeded benzene levels in water distribution systems after wildfires. To address the lack of predictive models, we developed and tested an approach based on neural network models to spatially predict the conditional probabilities of exceeding maximum contaminant levels for benzene after wildfires. The Bayesian regularized neural networks were trained using high-resolution data layers comprising topography, soil properties, landcover, vegetation, meteorological parameters, fuel load, and infrastructure data for two wildland urban interface areas in northern California. The generalized model ensemble encompassing data from both communities exhibits an accuracy of 83% to 88% in spatially predicting the post-fire exceedance of benzene levels, offering a planning tool for emergency response and future risk mitigation efforts.

## 1. Introduction

The risk and impact of wildfires has increased as a trend toward more frequent and more severe wildfires has been observed (Abatzoglou & Williams, 2016; Goss et al., 2020; Halofsky, Peterson, & Harvey, 2020; Higuera & Abatzoglou, 2020; Holden et al., 2018; Williams, Abatzoglou, Gershunov, et al., 2019). Contributing factors such as land use change and prolonged droughts associated with climate change are predicted to be more common in the future across western North America (e.g., Syphard et al., 2019; Ullrich et al., 2018) underlining the urgency to address risk factors to protect people, natural resources, and buildings.

Wildland-urban interface (WUI) areas, where structures and wildland vegetation meet or mix, are particularly prone to increased fire ignitions and impacts due to their proximity to large wildland fuel loads, increased human ignitions, and often increased distances to fire response facilities. Nevertheless, a continuous trend of extending

and increasing WUI areas has been observed in recent decades in the western US (Hammer, Radeloff, Fried, & Stewart, 2007; Radeloff et al., 2018).

Our study focuses on the cities of Santa Rosa and Paradise, two heavily sampled and studied WUI communities in northern California that were recently affected by wildfires. The Tubbs fire lasted from October 8 to 31 in 2017 and killed 22 people. It destroyed over 3100 structures. The extent of the Tubbs fire only reached the northern WUI section of the city of Santa Rosa. The Camp Fire lasted from November 8 to 25 of 2018. It caused 86 fatalities and burned more than 18000 structures. The fire spread through the entire area of the city of Paradise. The town of Paradise was almost completely destroyed. The fire displaced most of its 27 000 residents and 90% of its houses were lost to the fire (Chambers, Gorman, Feng, Torn, & Stapp, 2019). Beyond the loss of lives, the devastation of structures and vegetation, and high economic damage (Geller, 2018) in and around WUI areas, a very

\* Corresponding author.

E-mail addresses: [andres.schmidt@oregonstate.edu](mailto:andres.schmidt@oregonstate.edu) (A. Schmidt), [lisa.ellsworth@oregonstate.edu](mailto:lisa.ellsworth@oregonstate.edu) (L.M. Ellsworth), [jenna.tilt@oregonstate.edu](mailto:jenna.tilt@oregonstate.edu) (J.H. Tilt), [mike.gough@consbio.org](mailto:mike.gough@consbio.org) (M. Gough).

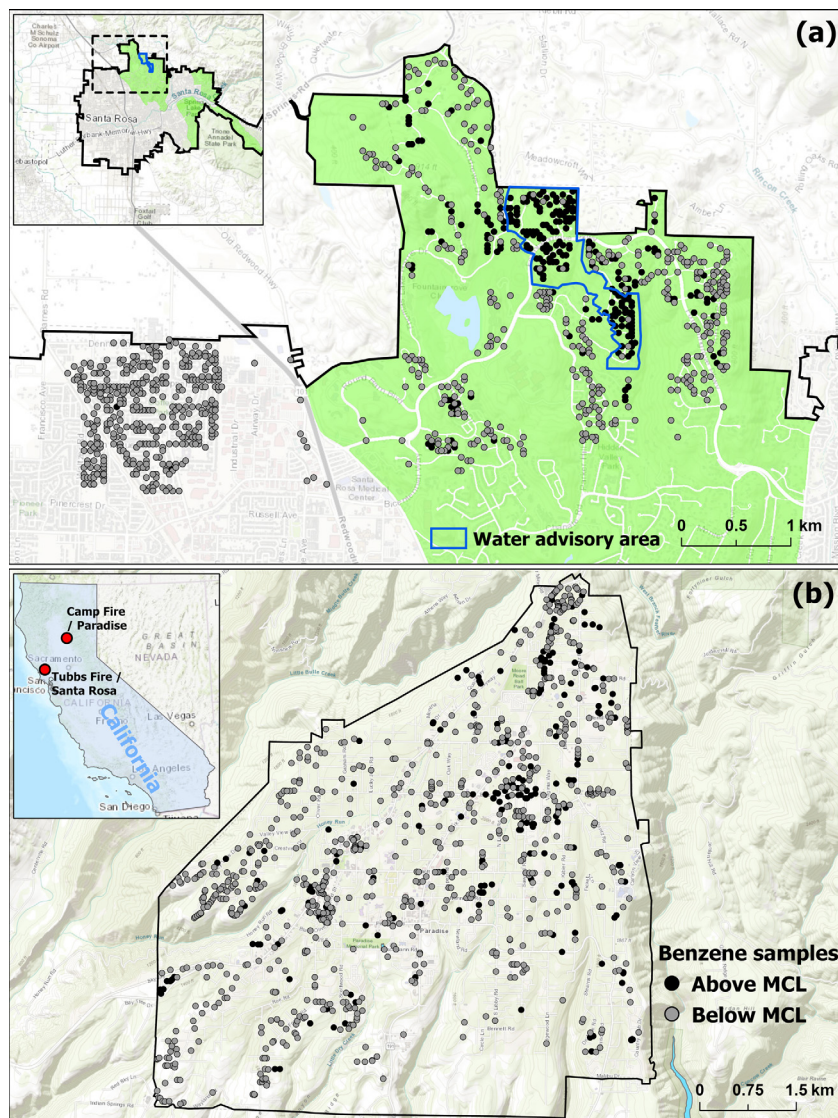


**Fig. 1.** Overview of study locations and classifications of drinking water samples taken in the areas that were affected by the 2017 Tubbs fire in the north of Santa Rosa (a) and the 2018 Camp Fire in Paradise (b), respectively. The green areas in panel (a) mark WUI zones as allocated by the city of Santa Rosa . (For interpretation of the references to color in this figure legend, the reader is referred to the web version of this article.)

recent discovery is the problem of harmful contaminants in drinking water distribution systems (WDS) after wildfires (e.g., Tolulope et al., 2021). The loss of structures to wildfires in California, as the most populous state in the US, is predicted to increase with expansion of rural residential land use and is highest in low housing density areas such as WUIs (Ager et al., 2021; Radeloff et al., 2018; Syphard et al., 2019).

Santa Rosa and Paradise were the first WUI communities for which the occurrence of water contaminants in their WDS after wildfires was reported and well-documented. In both towns, municipalities recorded increased levels of volatile organic compounds (VOCs) and semi-volatile organic compounds (SVOCs) after the wildfires, leading to severe health risks for the population (e.g., WHO, 1996). Benzene levels of samples in Santa Rosa exceeded the maximum contaminant level (MCL) of 1 µg/L for California by 4 orders of magnitude in some cases, and by 3 orders of magnitude in Paradise (Isaacson et al., 2021; Proctor, Lee, Yu, Shah, & Whelton, 2020). While fire damage to the WDS such as melted and burned pipes, valves, or water meters was noticed, some damage to the subterranean WDS is visually unnoticeable. Deformed and stressed water pipes and fittings can lead to water contamination as material from the surrounding substrate and runoff

can be introduced into the pipe system (e.g., Karim, Abbaszadegan, & Lechavallier, 2003; LeChevallier, Gullick, Karim, Friedman, & Funk, 2003; Proctor, Whelton, Shah, & Lee, 2021). Furthermore, synthetic plastic polymer-based water pipe material such as polyvinyl chloride (PVC) and high-density polyethylene (HDPE) can potentially release benzene and other VOCs when exposed to excessive heat during a fire at the surface, posing an additional way of contaminants being released into the drinking water system after fires (e.g., Chong, Abdulramoni, Patterson, & Brown, 2019; Proctor et al., 2020).

According to the National Primary Drinking Water Regulations (NPDWR), benzene levels are not to exceed 5 µg/L in drinking water because benzene is considered a carcinogen and poses a serious health risk if consumed by humans. In the state of California, the lower MCL is 1 µg/L. The City of Santa Rosa Water Department began testing water throughout their WDS after receiving complaints about the odor and taste of the water following the 2017 Tubbs Fire. Because concentrations measured at locations across the city exceeded both the lower California MCL of 1 µg/L and the federal EPA maximum contaminant level for benzene of 5 µg/L, the city of Santa Rosa issued a "Do Not Drink–Do Not Boil" advisory to a specific area of northern Santa Rosa after the fire in 2017 (Fig. 1a). Similarly, after the Camp

Fire in Paradise, 3800 addresses in Paradise were put under a water advisory because water samples exceeded the benzene MCL of 1 µg/L, in some cases by a factor of more than 2000. Values exceeding the MCL were still found up to 8 months after the wildfire at sample locations in Paradise and up to 11 months after the wildfire in Santa Rosa. The city of Paradise started to test water in January 2019 throughout the WDS. While various contaminants were found in the WDS of the two communities after the wildfires, we focus on benzene within this study because of its widespread and high abundance in the post-fire WDS samples of both locations. In addition, benzene is often used as a representative VOC contaminant in drinking water and detectable with standardized methods in corresponding chemical analyses (Zulkifli, Rahim, & Lau, 2018).

Measures of burn severity that are based on normalized difference vegetation index or differenced normalized burn ratio methods (e.g., Escuin, Navarro, & Fernández, 2008), as used for wildfire damage assessments to vegetation, are not suitable to detect structure damage in built-up areas or to detect contamination within a WDS (Schulze & Fischer, 2021). Moreover, current wildfire models do not allow for modeling burn probability or fire behavior in built-up areas due to a current lack of fuel models for such structures. Sections of built-up areas containing numbers of structures that can be close to burnable vegetation are currently classified as non-burnable in fuel layers of fire models (e.g., Picotte et al., 2019; Rollins, 2009). Hence, using a deterministic process model for spatial predictions of post-fire contamination risk with available sampling data and knowledge of processes, is currently unfeasible.

While post-fire assessments are crucial for recovery efforts, predictive models are needed to help WUI communities mitigate the risk of wildfire damage (McWethy et al., 2019), allocate resources, and protect critical infrastructure, such as the provision of drinking water. Further, knowledge of which areas are at risk would be valuable prior to a potential wildfire to guide suppression response and aid in post-fire recovery. However, mechanistic relationships between wildfire and water infrastructure damage are currently ill-defined as many contributing factors and processes are largely unknown and the corresponding data unavailable. In the WDS, processes such as the system-wide state of pressure, flow, and temperature in a complex pipe network across a town are unknown, except at certain main valves and control points. Furthermore, parameters change during wildfires when firefighting efforts or damaged pipes and associated pressure drops change flow rates and directions at one or many points of the WDS.

Recently, a functional relationship between the number of fire-damaged structures within a certain area and the probability of above MCL samples found in that area was estimated and described in Schulze and Fischer (2021) based on a simple fragility function. However, estimates based on this approach rely on post-fire damage assessment data for burned structures collected on the ground within 76 m (250 ft) around a sampling site making the approach unsuitable for pre-fire contamination risk predictions in high-resolution (such as the dwelling level).

Here, we present a machine learning approach using pattern recognition neural networks with classification output layers to spatially predict conditional probabilities of drinking water contamination in WUI areas after wildfires without the need for in-situ post-fire building damage assessments. We use analytical results of post-fire water samples, topographic factors, landcover data, information about infrastructure, and physical soil properties in combination with Bayesian regularized neural networks to develop network ensemble models that predict conditional probabilities for benzene levels in WDS exceeding the MCL. To the knowledge of the authors, this is the first predictive model addressing the contamination probability of drinking water from WDS after a potential wildfire. The models can be used for planning purposes in other WUI areas, to pre-allocate resources after possible wildfires, and prevent the consumption of drinking water from WDS with increased benzene levels that pose a significant health threat for humans.

## 2. Data and methods

### 2.1. Water sample data

All water sampling data used within this study were provided by the Paradise Irrigation District (PID) and the Santa Rosa Water Department (SRWD). The water sampling data include the location of the sample, the names and concentrations of contaminants found in the sample, and whether the sample exceeded the respective California MCL for drinking water. 1168 water samples were available in the city of Santa Rosa to train the networks. Across the city of Paradise, a total of 1078 water samples were available (Fig. 1).

Building codes for utility lines differ based on region, year, surface composition, and infrastructural factors. However, generally, water service lines are buried relatively close to the surface (ca. 0.50 m depth) while main water pipelines are installed deeper in the ground (>1.3 m depth) where they are protected from elevated temperatures and associated damage through wildfire. Thus, main distribution lines experienced only minimal contamination (3% of main pipelines tested exceeded the MCL in Santa Rosa and Paradise, respectively, whereas almost 20% of the samples taken from service lines had benzene concentration that exceeded the MCL (Schulze & Fischer, 2021)). Hence, only water sampling results from service lines were used for our analyses. Samples taken after the fires with benzene levels above 1 µg/L are hereafter referred to as ‘contaminated’ or ‘positive’ and were assigned a value of 1 in the data record whereas samples with 1 µg/L and below are referred to ‘non-contaminated’ or ‘negative’ and were assigned a value of 0 for the classification training of the neural networks. Several locations where above MCL concentrations were found were sampled multiple times over several months to observe the water quality after flushing of the system or replacement of pipes, valves, or meters within the WDS. Hence, those locations had positive and negative contamination statuses assigned at different sample dates. Such points were classified as contaminated for the network training if any of the samples after the wildfire exhibited a benzene concentration >1 µg/L.

To account for the imbalanced data class distribution (26% of all samples are above the MCL and 74% within the MCL limit), we applied random under sampling to the datapoints below or at the MCL during the Bayesian regularized network training runs to mitigate the effect of the slightly imbalanced datasets (e.g., Bach, Werner, & Palt, 2019; Buttijak, Suchatpattmakul, Suksirisopak, & Suwansantisuk, 2020; Devi, Biswas, & Purkayastha, 2020; López, Fernández, García, Palade, & Herrera, 2013). Furthermore, we assessed model performances through class-specific errors based on confusion matrices, considering not only overall accuracy (or error) but specifically false positive, and false negative test error values.

### 2.2. Model input data

All input data variables were aggregated to 30 × 30 m spatial resolution covering the 15 km × 15 km model domains with the cities Santa Rosa and Paradise in their centers covering all sample points and their surroundings across the two study areas. With the sampling locations included, this provides 250 000 datapoints for each input variable for the application of the model.

For the topographic data layers, we used the 30 m NASA Shuttle Radar Topography Mission dataset (SRTM, Farr et al., 2007) version 3.0. Aspect values were calculated using the ESRI ARCGIS Surface Parameters tool with adaptive neighborhood selection and quadratic surface functions fitted around each grid cell (e.g., Wilson & Gallant, 2000; Zevenbergen & Thorne, 1987). Vegetation fuel load was quantified through landcover type, percentage vegetation cover, and vegetation height. We used the LANDFIRE 2016 Remap (LF 2.0.0) for existing vegetation height (EVH) and percentage vegetation cover. The Multi-Resolution Land Characteristics Consortium (NLCD 2016) dataset was used for landcover type classification. Distance to the closest

grid cell with vegetation cover  $\geq 50\%$  was provided for each sample point. To account for the potential structural fuel load in WUIs in addition to the vegetation fuel load, building density was calculated in buildings per hectare as information for the networks. The locations of buildings were taken from the 2018 Microsoft Building Footprint data that was created from satellite and aerial imagery using the ResNet34 deep neural network (Heris, Foks, Bagstad, Troy, & Ancona, 2020). The spatial values for contents of clay, silt, and sand, as well as soil bulk density were downscaled using the WoSIS (Batjes, Ribeiro, & van Oostrum, 2020) and SoilGrids datasets publicly provided through [soilgrids.org](http://soilgrids.org) and described in Hengl et al. (2017) and Poggio et al. (2021). Locations of fire stations were obtained from the Homeland Infrastructure Foundation-Level Data database (HIFLD, Foster & Mayfield, 2016) and distances to the nearest fire station were calculated for each grid cell and sample point.

To account for the influence of wind on wildfire behavior and intensity (Mass & Ovens, 2019; Quill, Sharples, Wagenbrenner, Sidhu, & Forthofer, 2019; Rodman, Winterkamp, Edminster, Colman, & Smith, 2017) we used the average predominant wind directions and wind speeds as reported during the fires in Santa Rosa and Paradise, respectively. The wind fields were then downscaled with WindNinja (ver. 3.7.2, Wagenbrenner, Forthofer, Lamb, Shannon, & Butler, 2016) to account for topography and surface roughness and obtain the 30 m resolution wind fields for the two model domains. The thermal conductivity of soil has a strong effect on the resulting belowground temperature and, hence, the heat-related pipeline damage from above-ground fire potentially causing deformation, melting, and heat-induced release of contaminants in belowground water pipes. Using the soil data from the SoilGrids repository in combination with average soil moisture values during the months of the fire occurrences from the TerraClimate database (Abatzoglou, Dobrowski, Parks, & Hegewisch, 2018), we spatially calculated the thermal conductivity  $k$  following Bertermann, Müller, Freitag, and Schwarz (2018) with,

$$k = 0.1442 \times (0.7 \times \log(\Theta/\rho) + 0.4) \times 10^{0.6243\rho} \quad (1)$$

for soils that contain more than 50% sand. Eq. (1) is adjusted for soils that contain more than 50% silt as given through Eq. (2),

$$k = 0.1442 \cdot (0.9 \cdot \log(\Theta/\rho) - 0.2) \cdot 10^{0.6243\rho}. \quad (2)$$

Here,  $\rho$  is the soil bulk density and  $\Theta$  denotes the volumetric water content, derived from the SoilGrids and TerraClimate database, respectively.

All input variables were scaled to a range between 0 and 1 for the training of the neural networks to account for the different orders of magnitude of the variables and corresponding units. Directional values (aspect and wind direction) in degrees from north were reclassified to make the circular value range more suitable for network training. The discretization also accounts for the generally higher fire risk associated with easterly winds compared to other wind directions in our study region (e.g., Jin, Scaduto, & Chen, 2019; Keeley & Syphard, 2019).

While building materials, age of structures, and pipeline material potentially may influence the fire-induced risk of MCL exceedance, such information was not comprehensively available for our data points. Furthermore, our model aims to predict the conditional (after a fire occurred) probability of benzene MCL exceedance, in WUI areas spatially, including locations where no buildings exist yet but are deemed suitable for extension of housing. Thus, data that exclusively pertains to individual buildings were not used for the model training.

### 2.3. Theory of Bayesian regularized networks applied to the datasets

The advantage of a neural network model over a mechanistic process model is that no prior knowledge about functional relationships between the driving input variables and the target variable is needed (e.g., Bishop, 2006). Thus, no model-simplifications that constrain the outcome by the number of available algorithms and corresponding parametrizations are required. This makes neural networks particularly

suitable for our study because contributing factors and exact processes that lead to water contamination after wildfires are not understood comprehensively and, accordingly, no process models were available at the time this study was conducted.

Neural networks, along with other machine learning methods, have been successfully applied for wildfire vulnerability and susceptibility assessments (de Bem, de Carvalho, Matricardi, Guimarães, & Gomes, 2018; Zhang, Wang, & Liu, 2019), burned area segmentation (e.g., Knopp, Wieland, Rättich, & Martinis, 2020), wildfire risk predictions (Malik et al., 2021), and various other fields of wildfire research over the last three decades (Jain et al., 2020).

Here, we used shallow pattern recognition neural networks with sigmoid transfer functions in the hidden layer and SoftMax transfer functions in the classification output layer to separate the water sample data into “above MCL” or “below MCL” (including “at MCL” which did not occur in dataset used) and calculate corresponding class assignment probabilities. The model is based on driving input variables that pertain to fuel load availability, fire severity, and heat transfer through soil. The trained networks used input vectors composed of different predictive variables and consist of 40 to 80 neurons in the hidden layer and a SoftMax output layer to assign allocation probabilities to each classification output.

Bayesian regularization was applied for the training procedure to better facilitate the use of noisy data or maximize the utilization of limited amounts of available training data (Burden & Winkler, 2009; Schmidt, Creason, & Law, 2018; Schmidt, Mainwaring, & Maguire, 2020). The Bayesian regularization technique uses the Levenberg–Marquardt minimization algorithm to minimize a linear combination of squared errors using a gradient technique to determine network parameters, resulting in a network with strong generalization capabilities mitigating potential over-adjustment to available training data (Burden & Winkler, 2009; Foresee & Hagan, 1997). Bayesian regularization also eliminates the need for a validation data subsample which reduces the amount of data needed for the network model learning process. This is an advantage over the cross-validation approach in gradient-based backpropagation algorithms if available training data are limited as is the case for our study.

The mean squared error  $E$  between the samples and the corresponding network output was used as performance function for the network training. By adding a penalty term to the network optimization algorithm, the method reduces the potential for over-adjustment of the network to the training data by enhancing the error function and set the number of weights as an optimization goal. For that purpose, the sum of squares of the network weights  $E_w$  (Eq. (3)) is added to the error function. Here,  $w_j$  is the  $j$ th element of the weight vector  $w$  of length  $n$ , and  $\alpha$  and  $\beta$  are performance function weight parameters between 0 and 1:

$$E_w = \frac{1}{n} \sum_{j=1}^n w_j^2, \quad (3)$$

where  $w_j$  is the  $j$ th element of the weight vector  $w$  of length  $n$ . This provides an error-dependent cost function  $F$  that also accounts for network weight minimization, as given in Eq. (4):

$$F = \alpha E_w + \beta E, \text{ with } \alpha + \beta = 1, \quad (4)$$

with  $\alpha$  and  $\beta$  referring to performance function weight parameters that exhibit values between 0 and 1. By reducing the number of effective weights to an optimized number, the sum of the network weights is limited, allowing the network to match the inputs to the training targets while also restricting network complexity. This improves the network's generalization when faced with new data by making the network's response to the presented inputs smoother and less prone to over-fitting.

The cost function weight parameter  $\beta$  sets the emphasis of the training algorithm toward reducing the network error term  $E$ , whereas increasing parameter  $\alpha$  reduces the sum of the weights integrated

over all network neurons. The minimization of the network errors (i.e., minimization of the cost function (Eq. (4)) was achieved using the Levenberg–Marquardt (LM) optimization algorithm as implemented in Matlab (R2021a). The LM method was used as the iterative numerical standard approach to solve non-linear minimization problems, combining the gradient-descent method and the Gauss–Newton minimization algorithm (Butenko & Pardalos, 2014; Marquardt, 1963). The adaption of the network weights during the LM iteration and the search for the optimal number of active weights were regularized using a Bayesian approach following MacKay (1992).

The posterior of the probability density function is maximized using Bayes' rule:

$$P(d|\alpha, \beta, M) = \frac{P(d|\mathbf{w}, \beta, M) \cdot P(\mathbf{w}|\alpha, M)}{P(\mathbf{w}|d, \alpha, \beta, M)}. \quad (5)$$

Here,  $d$  is the available dataset with inputs and targets,  $M$  is the network model, and  $\mathbf{w}$  is the vector of neural network weights. Assuming a Gaussian distribution for the random noise in the training data and for the prior distribution of the network weights that are, in fact, initialized randomly in the algorithm, the probability terms in the numerator can be substituted through,

$$P(\mathbf{w}|\alpha, M) = \frac{1}{Z_w(\alpha)} \exp(-\alpha E_{\mathbf{w}}) \quad (6)$$

and

$$P(d|\mathbf{w}, \beta, M) = \frac{1}{Z_d(\beta)} \exp(-\beta E), \quad (7)$$

and Eq. (5) can be written as:

$$P(d|\alpha, \beta, M) = \frac{\left[ \frac{1}{Z_d(\beta)} \exp(-\beta E) \right] \left[ \frac{1}{Z_w(\alpha)} \exp(-\alpha E_{\mathbf{w}}) \right]}{\frac{1}{Z_F(\alpha, \beta)} \exp(-F(\mathbf{w}))} = \frac{Z_F(\alpha, \beta)}{Z_w(\alpha) \cdot Z_d(\beta)}, \quad (8)$$

with  $Z_d(\beta) = (\pi/\beta)^{n/2}$  and  $Z_w(\alpha) = (\pi/\alpha)^{N/2}$ .

After approximating  $Z_F$  through a Taylor series, solving for the denominator in Eq. (8) we get:

$$Z_F \approx (2\pi)^{N/2} (\det((\mathbf{H}^{MP})^{-1}))^{1/2} \cdot \exp(-F(\mathbf{w}^{MP})), \quad (9)$$

where  $MP$  indicates the minimum point of the cost function or the maximum posterior of the probability density  $P(d|\alpha, \beta, M)$ , respectively.  $\mathbf{H}$  is the Hessian matrix of the cost function containing the second order partial derivatives of  $F(\mathbf{w})$ .

Substituting  $Z_F$  in Eq. (8) by the approximation of Eq. (9) and setting the first derivative of Eq. (8) equal to zero yields the values for the weight parameters at the minimum of the cost function:

$$\alpha^{MP} = \frac{\mu}{2E_{\mathbf{w}}(\mathbf{w}^{MP})} \quad (10)$$

And

$$\beta^{MP} = \frac{n - \mu}{2E(\mathbf{w}^{MP})} \quad (11)$$

$$\text{with } \mu = N - 2\alpha^{MP} \text{Tr}(\mathbf{H}^{MP})^{-1}. \quad (12)$$

Here,  $\mu$  is the minimized effective number of parameters in the optimized network and gives the number of parameters in the network that were effectively used to minimize  $F$ .

$Tr$  represents the trace of the inverse Hessian matrix  $\mathbf{H}$  at the minimum point ( $MP$ ) of the cost function equation (Eq. (12)).

All networks used within this study were trained until the sum-squared error, the sum-squared weights, and the effective number of parameters converged at their optima. Initial values of  $\alpha$  and  $\beta$  were set to 0.5, equalizing the priority of  $MSE$  minimization and the minimization of the mean squared sum of the weights at the beginning of the learning process. We trained individual models using solely the data from Santa Rosa or Paradise, respectively. In addition, a generalized

model was trained combining the datasets from both sites. For each model 15% of the data was randomly chosen as the test dataset not included in the network training was ended after 100 epochs when the training errors converged. If the functional relations and, hence, the ideal set of input variables is unknown, the use of too many variables leads to a deterioration of the network model performance. Instead of adding useful information the correlation between observed and modeled test data starts to decrease. This undesirable consequence is caused by the increasing dimensionality of the cost function to be minimized (Eq. (3)) which makes finding the global error minimum more difficult (e.g., Bengio & Bengio, 2000; Bishop, 2006; Haykin, 2009). A schematic of the training processes for the Bayesian regularized classification networks and methods applied is given in Fig. 2.

Using random numbers of input variables from 8 to 16 and combinations of the input variables allows for 39 203 possible input vector compositions. For each dataset (Santa Rosa, Paradise, and combined data) we ran 40 000 simulations with no repetitions allowed and recorded the error values. Performances were assessed with respect to three errors: The overall test error for samples assigned to the wrong class, the false negative error ('above MCL' samples misclassified as 'non-contaminated'), and the false positive error ('below MCL' samples misclassified as 'contaminated') based on the class assignment probabilities between 0 and 1 of the SoftMax function signal in the output layer. We used ensembles combinations that minimized the combination of all three test errors to improve overall accuracy (e.g., Haro-García, Cerruela-García, & García-Pedrajas, 2020; Polikar, 2012) and applied the ensembles to both study sites with continuous spatial coverage. This iterative optimization procedure was independently applied for each site-specific model and for the generalized model that was trained using all sample data from all test sites combined.

### 3. Results and discussion

Fig. 3 shows the averages of the input variables at the sampling points rescaled to a range from 0 to 1 for the network training. Most averages across the positive and negative samples are close and patterns differ across the two study sites with no simple linear correlations visible that clearly distinguish above MCL samples from below MCL samples at either site. Nevertheless, several site characteristics are reflected in the data.

The results in Santa Rosa (Fig. 3a) show that more samples exceeding the California benzene MCL were found in higher elevation locations compared to the negative (below MCL) samples that were predominantly found in areas of the city that exhibit a flat landscape at lower elevation.

This corresponds to the WUI area in the elevated hills of the northeastern part of Santa Rosa (Fig. 1a) that exhibited a higher burn severity according to the MTBS data record (Schulze & Fischer, 2021) as well as increased benzene levels after the fire.

Similarly, the mean building density in the urban residential outskirts in the northwest, where mostly samples with benzene concentrations below the California MCL were found, exhibits roughly twice the building density of the northeastern WUI area in Santa Rosa, whereas the respective difference is comparatively small (16%) and within the  $1\sigma$ -range for the samples in Paradise with its homogeneously low building density across town.

This also applies to the distance to the nearest vegetation (with at least 50% coverage) that separates the WUI area in Santa Rosa from the more urban outskirts, while there is no significant difference in the corresponding averages for Paradise (Fig. 3). The clusters of elevated benzene concentrations exceeding the respective MCL are recognized by the model with some grid cells where no houses existed yet also being assigned high conditional probabilities.

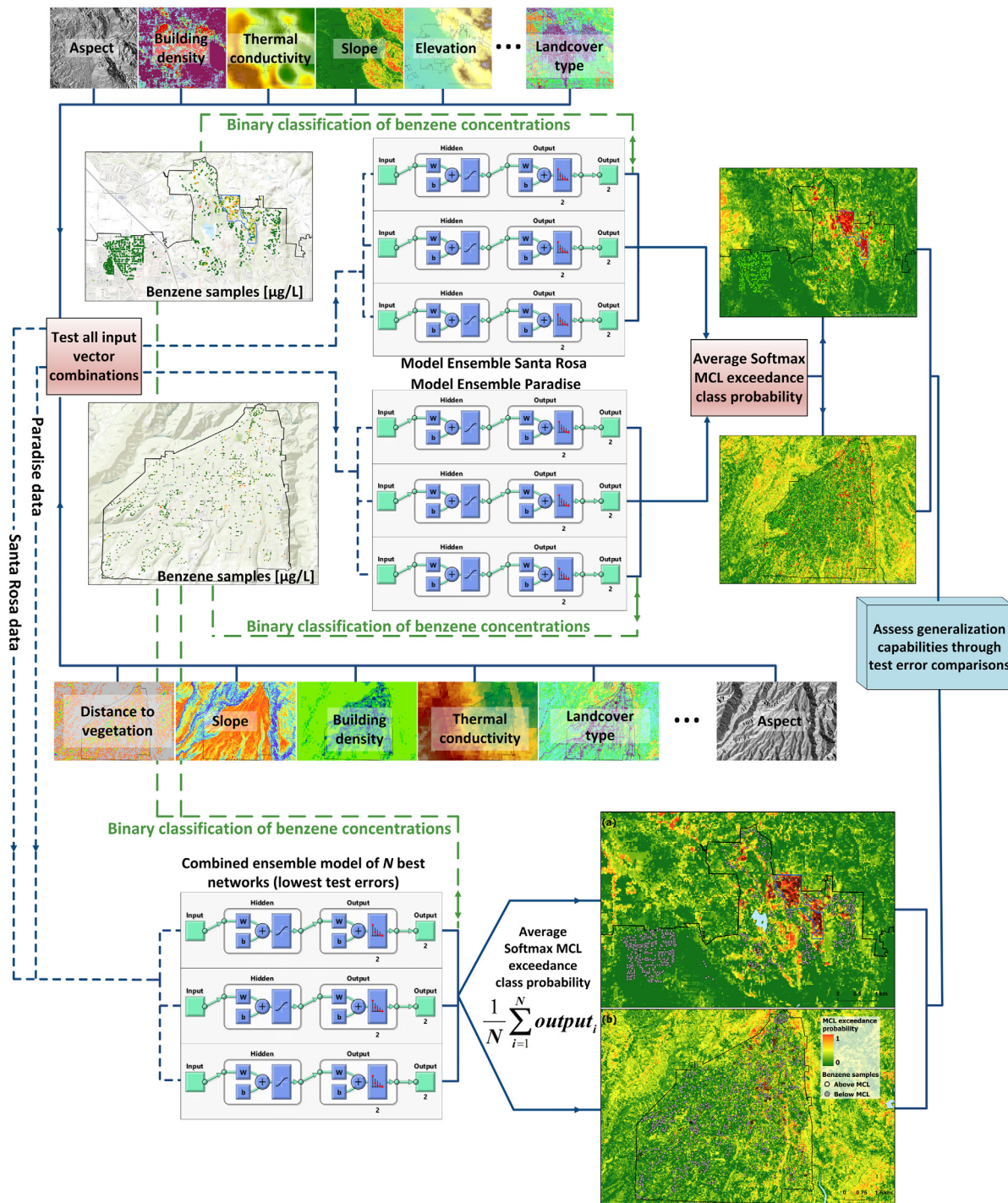


Fig. 2. Schematic of the processes for the combined network ensemble optimization.

### 3.1. Network response analyses

To assess the sensitivity of the non-linear neural network outputs to the input variables we compared the test errors using specific input vector combinations. Starting with all 16 variables used as inputs we calculated the test error averaged over the outputs of 1000 network models trained with both datasets merged as used for the final combined ensemble network. For each group of 1000 networks, a specific variable was removed from the input vector and the average test error was calculated. Finally, the average test error for the networks including all variables was then subtracted from the errors calculated with every variable consecutively removed from the input to determine the

percentage changes of the test errors. The result of the response analysis (Fig. 4) show that most test errors varied most predominantly with EVH, percentage vegetation cover, and building density, respectively. Due to non-linearity of the functional relationship between the input and output mapped by the networks it should be noticed here that the exclusion approach only reflects the test error responses specific to the exclusion of one specific variable without considering the potential of this variable to change the network output in combination with other variables.

Hence, while this shows responses of the training error reaching  $\pm 13\%$  for some networks (Fig. 4) it cannot be interpreted as a simple importance measure of any variable because the interdependencies

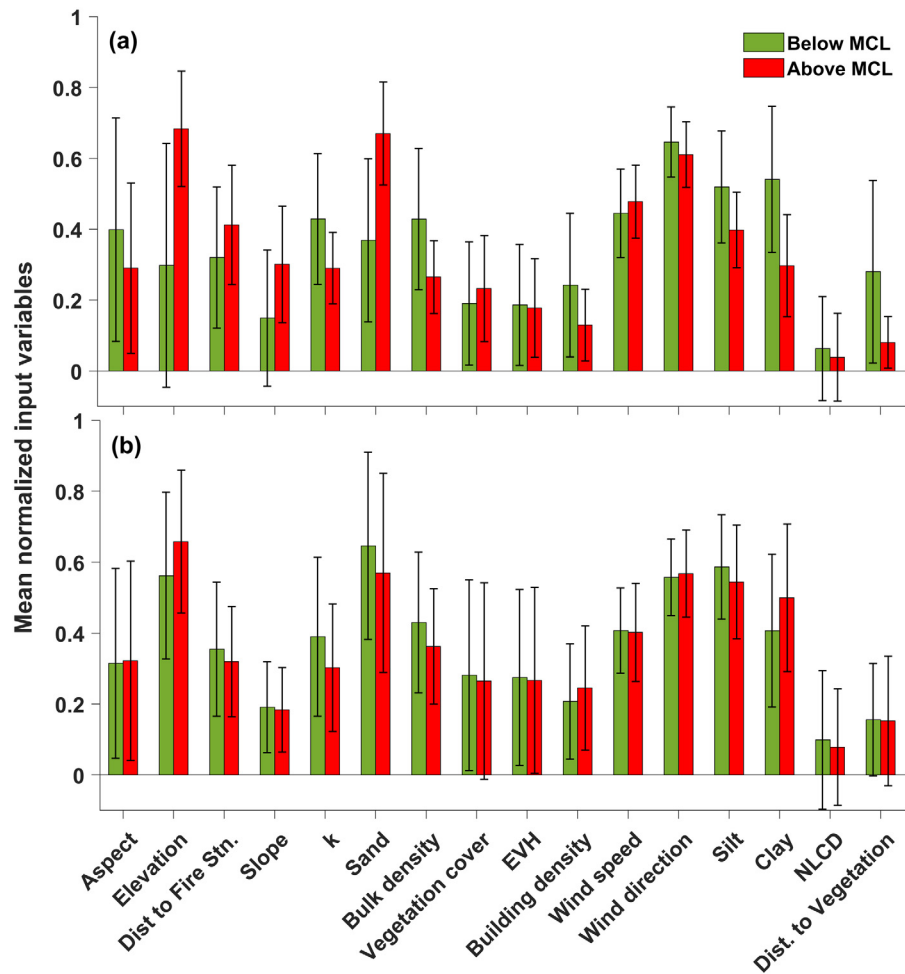


**Fig. 3.** Averages of the normalized input variables for the available training data samples in Santa Rosa (a) and Paradise (b). The black bars mark the  $1\sigma$  ranges over all positive (red) and all negative (green) sample locations. (For interpretation of the references to color in this figure legend, the reader is referred to the web version of this article.)

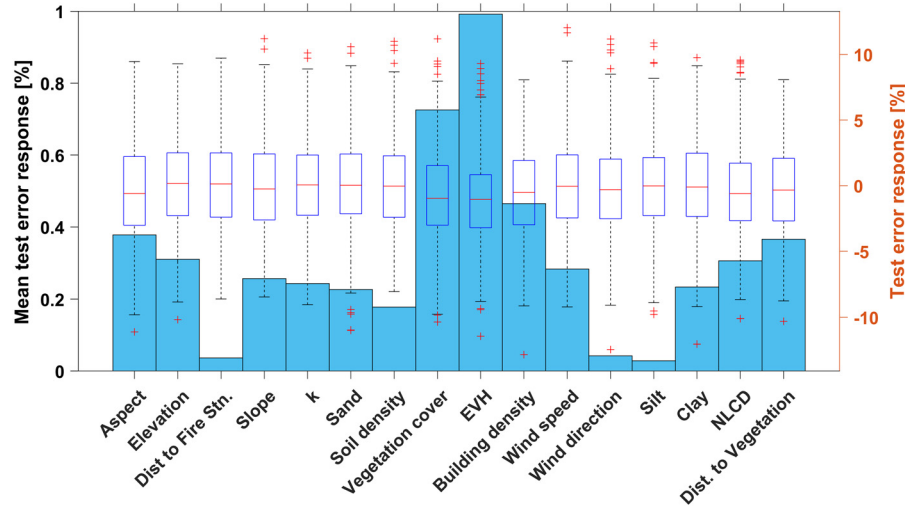


**Fig. 4.** Absolute mean differences (blue bars, left y-axis) between the average test errors using input vectors without a specific variable and the test error when all 16 variables are used and the corresponding box-whisker plots (right y-axis). All values are calculated for 1000 network outputs, independently for each of the 17 input vector compositions. (For interpretation of the references to color in this figure legend, the reader is referred to the web version of this article.)

between the variables of any variable combination are not considered in this analysis. This means, for instance, while the test error responses with the wind direction excluded differ only slightly, wind directions could still strongly affect the results in combination with a specific set of input variables and reinforce or mitigate the effect of those variables.

### 3.2. Site-specific model results for Santa Rosa

The network ensemble model based on the Santa Rosa data manages to simulate the distinguished zones of samples with high benzene concentrations in the northeastern region of the city where large parts

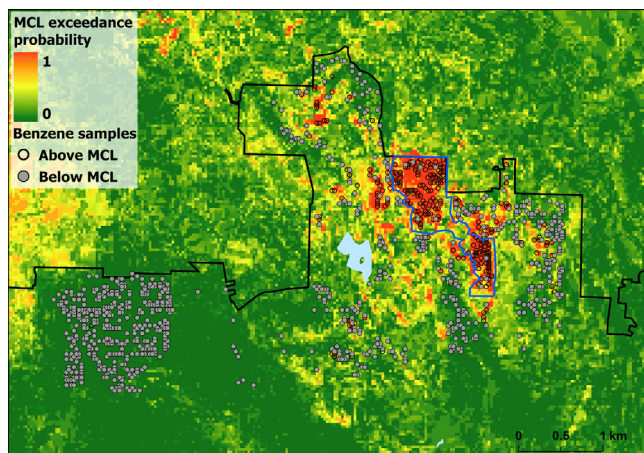


**Fig. 5.** Spatial distribution of MCL exceedance probabilities after a fire event using a site-specific model ensemble for Santa Rosa. The blue outline marks the water advisory area declared by the city of Santa Rosa after the fire in 2017. (For interpretation of the references to color in this figure legend, the reader is referred to the web version of this article.)

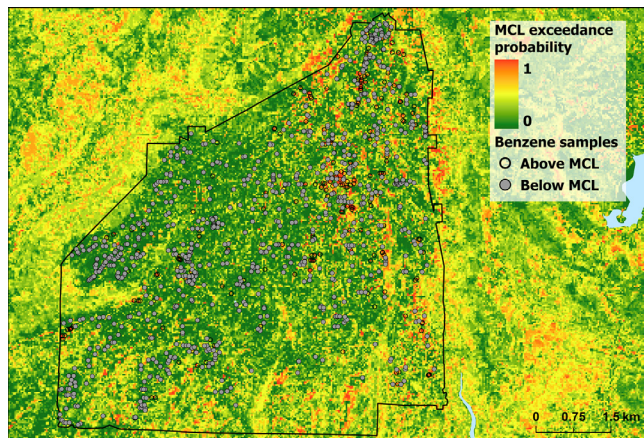


**Fig. 6.** Spatial distribution of MCL exceedance probabilities after a fire event using a site-specific model ensemble for Paradise.

of the agglomeration of samples significantly exceeding the MCL was enveloped by a water advisory area along with some negative samples. Furthermore, in the most northern region of the city limits, some small areas with positive samples are visible and the high probabilities were classified accordingly by the networks in those areas as shown in Fig. 5.

The sample results in Santa Rosa clearly represent the WUI area located in the elevated and forested region in the northeast and the more urban, densely built-up outskirts in the northwestern part of the city where only a few positive samples were observed (Figs. 1 and 5).

### 3.3. Site-specific model results for Paradise

The spatial distribution of positive and negative samples in Paradise is less clearly clustered, compared to the samples in the Santa Rosa area. While some areas show agglomerations of positive samples, those areas are scattered across the entire town and are close to negative samples across the city area. One explanation is the layout of the city that differs from the site in Santa Rosa where the fire only affected the northern part of the city. In Paradise, the Camp Fire of November 2018 swept across the entire city area from northeast to southwest. Furthermore, while the city of Santa Rosa only exhibits patterns of a WUI area in the northern outskirts of town, the town of Paradise showed classical characteristics of a WUI area with dense vegetation

**Table 1**

Topology and input vector composition of the best network models and corresponding ensembles used to create the final MCL exceedance probability maps. A topology such as 16-42-2 symbolizes 16 input variables, 42 neurons in the hidden layer and 2 classes in the output layer.

Network model ensemble	Network topologies	Variables excluded from input vector
Santa Rosa data	16-42-2	–
	14-54-2	Soil density, clay content
	12-44-2	Sand content, soil density, wind speed, NLCD
	15-66-2	Wind speed
	14-58-2	k, wind speed
	12-57-2	Elevation, slope, vegetation cover, EVH
Paradise data	13-75-2	Elevation, wind direction, clay content
	14-75-2	Sand content, clay content
	12-75-2	dist. to fire station., slope, silt, NLCD
	13-72-2	dist. to fire station., slope, wind speed
	15-71-2	Silt
	16-74-2	–
Combined generalized model	14-70-2	k, dist. to vegetation
	14-56-2	elevation, sand content
	14-46-2	dist. to fire station., silt content
	15-50-2	k
	13-63-2	Aspect, slope, EVH
	14-63-2	Vegetation cover, silt content
	16-66-2	–
	15-58-2	Sand content

**Table 2**

Percentage test errors and class-specific test errors for the network ensemble models.

		Test error (%)	Test Error (%)	Test error (%)
		Overall	(false negative)	(false positive)
Specific models	Santa Rosa	6.89	10.69	5.36
	Paradise	10.38	15.29	8.49
Combined model	Santa Rosa	7.85	12.35	5.93
	Paradise	14.78	16.90	13.64

cover throughout the city limits embedded in a large area of forest and grassland around the town. The agglomerations were clearly simulated by the model showing high probabilities gradually decreasing with distance from the patches affected by benzene levels above the MCL (Fig. 6).

In combination with the minimization of the cost function (Eq. (4)) during the Bayesian regularized learning, more data with more variability increases the generalization capabilities of the model. Therefore, we combined the datasets and trained more generalized neural network models (Table 1) and applied the combined model ensemble to 15 km × 15 km areas with 30 m × 30 m spatial resolution covering both study areas.

### 3.4. Generalized model results with combined datasets

Using the generalized combined network ensemble models, the specific errors in Santa Rosa and Paradise only slightly increase (Table 2) indicating that the site-specific models capture the functional relationship between the input variables and the target data and significant overadjustment to the specific site data was successfully prevented by the Bayesian regularization process. Furthermore, the combined model ensemble generalizes sufficiently across the two available datasets with an overall test error for the combined model of 7.85% and 14.78% for Santa Rosa and Paradise, respectively.

The spatial distribution of the conditional post-fire MCL exceedance probabilities presented in Fig. 7 exhibit larger scale patterns similar to the networks trained with the site-specific data only (Figs. 5 & 6). In Santa Rosa, the highly affected WUI zone in the northeast with high MCL exceedance probabilities and the lower impacted residential area in the northwestern outskirts with exceedance probabilities from 0%

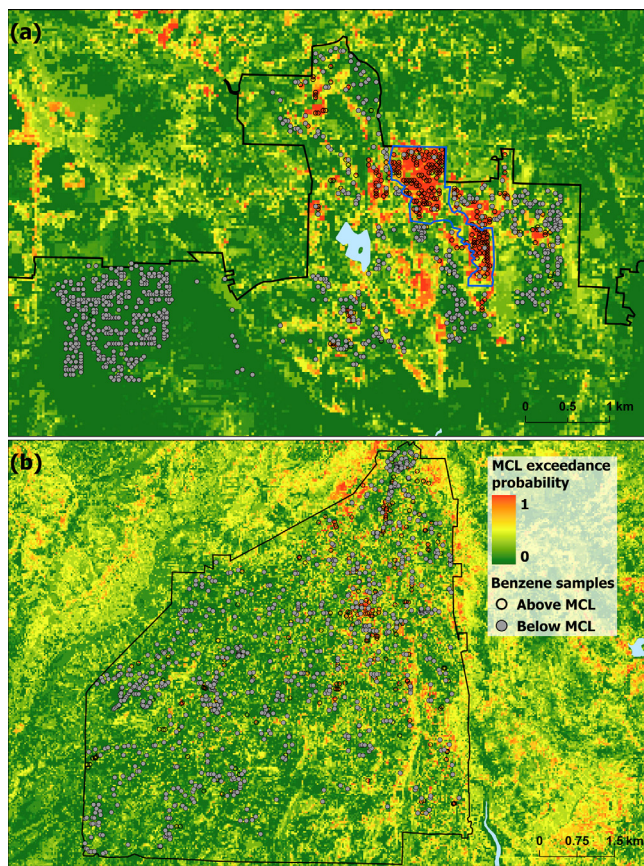


**Fig. 7.** Spatial distribution of MCL exceedance probabilities after a fire event for Santa Rosa (a) and Paradise (b) based on the combined dataset and model ensemble.

to 54% are clearly mapped by the combined network ensemble. On the smaller scale some differences between the site-specific model based on Santa Rosa data only and the general model are visible. The only two samples of the data used that showed benzene concentrations above the MCL in the northwest low-risk cluster in Santa Rosa were classified with 0.1% and 53.6% exceedance risk, respectively, while all other points were correctly assigned values significantly lower than 50%.

The MCL exceedance probabilities 0.26% to 99.9% with an average of 72.6% for the grid cells delineated by the water advisory area. Using a two-sample Kolmogorov-Smirnov test, the two value distributions distribution within the advisory area represent the same continuous distribution on a 95% confidence level, showing the close agreement of the general model and the model based on the Santa Rosa training data only. The similarity of the specific data model results and the combined model results suggests that the single-site results are not over-adjusted to the limited available datasets. As more data on drinking water contamination becomes available, the model can be trained and generalized and applied in areas with significantly different environmental conditions (i.e., landcover, land use, meteorology, and topography).

#### 4. Conclusion

Our machine learning approach achieves high accuracies partially exceeding 90% combined with good generalization capabilities if data pertaining to wildfire risk and heat-related damage susceptibility of underground pipe systems are used. Thus far, due to limited available WDS data samples, the models are suitable for regions that exhibit a similar range of conditions regarding predictive variables that describe topography, meteorology, soil, land use, and landcover. Nevertheless,

considering the spatial constraints associated with a novel and likely growing future dataset, the methods presented here can be applied for resource allocation or mitigation of drinking water contamination risk through wildfires prior to an incident to support decision makers and incident managers with WDS contamination probabilities.

For future studies, more post-fire WDS samples will be available as the recognition of the problem likely encourages affected WUI communities as well as WDS managers and operators to conduct post-wildfire drinking water sampling. The methodology could be enhanced by including image analysis that accounts for the surrounding of the sample point instead of values restricted to a single location of the water sampling. Remote sensing resources could be applied for in-situ risk assessments of WUI areas threatened by potentially spreading wildfires. For that purpose, deep neural networks could capitalize on more available and more complex data and potentially increase the predictive capacity through decomposition of more complex imagery data compared to shallow network models. Furthermore, socio-economic data could be included in subsequent analyses to spatially assign resources, benefitting areas that are more vulnerable and exhibit low recovery potential after wildfire damages to the WDS occur due to low income or insufficient insurance coverage, for instance. Finally, improvement of WUI fuel models to incorporate both structures and wildland fuel components may help elucidate the role that fuel arrangement, loading, and structure play in post-fire WDS damage.

#### Declaration of competing interest

The authors declare that they have no known competing financial interests or personal relationships that could have appeared to influence the work reported in this paper.

#### Acknowledgments

This research was funded by the Alfred P. Sloan Foundation, United States [Grant number: G-2019-12450]. The authors also would like to thank the cities of Santa Rosa and Paradise for the provision of various spatial datasets and the Paradise Irrigation District and the Santa Rosa Water Department for providing the post-fire water sampling results. The authors also would like to thank the SRTM project, HIFLD, SoilGrids, TerraClimate, and LANDFIRE for providing data used in this study and making it easily available for research through their web repositories and personnel.

#### References

- Abatzoglou, J. T., Dobrowski, S. Z., Parks, S. A., & Hegewisch, K. C. (2018). Terracimate, a high-resolution global dataset of monthly climate and climatic water balance from 1958–2015. *Science and Data*, 5, 170–191. <http://dx.doi.org/10.1038/sdata.2017.191>.
- Abatzoglou, J. T., & Williams, A. P. (2016). Impact of anthropogenic climate change on wildfire across western US forests. *Proceedings of the National Academy of Sciences of the United States of America*, 113, 11770–11775. <http://dx.doi.org/10.1073/pnas.1607171113>.
- Ager, A. A., Day, M. A., Alcasena, F. J., Evers, C. R., Short, K. C., & Grenfell, I. (2021). Predicting paradise: Modeling future wildfire disasters in the western US. *Science Total Environment*, 784, Article 147057. <http://dx.doi.org/10.1016/j.scitotenv.2021.147057>.
- Bach, M., Werner, A., & Palt, M. (2019). The proposal of undersampling method for learning from imbalanced datasets. *Procedia Computer Sciences*, 159, 125–134. <http://dx.doi.org/10.1016/j.procs.2019.09.167>.
- Batjes, N. H., Ribeiro, E., & van Oostrum, A. (2020). Standardised soil profile data to support global mapping and modelling (WoSIS snapshot 2019). *Earth Systems Science and Data*, 12, 299–320. <http://dx.doi.org/10.5194/essd-12-299-2020>.
- de Bem, P. P., de Carvalho, J. O. A., Matricardi, E. A. T., Guimarães, R. F., & Gomes, R. A. T. (2018). Predicting wildfire vulnerability using logistic regression and artificial neural networks: a case study in Brazil's federal district. *International Journal of the Wildland Fire*, 28, 35–45. <http://dx.doi.org/10.1071/WF18018>.
- Bengio, S., & Bengio, Y. (2000). Taking on the curse of dimensionality in joint distributions using neural networks. *IEEE Transaction on Neural Networks Special Issue on Data Mining and Knowledge Discovery*, 11, 550–557.

- Bertermann, D., Müller, J., Freitag, S., & Schwarz, H. (2018). Comparison between measured and calculated thermal conductivities within different grain size classes and their related depth ranges. *Soil Systems*, 2. <http://dx.doi.org/10.3390/soilsystems2030050>.
- Bishop, C. M. (2006). *Pattern recognition and machine learning* (1st ed.). (p. 738 pp). New York: Springer.
- Burden, F., & Winkler, D. (2009). Bayesian regularization of neural networks. In *Artificial neural networks: methods and applications* (Livingstone, D. J.). (pp. 23–42). Totowa, NJ: Humana Press.
- Butenko, S., & Pardalos, P. M. (2014). *Numerical methods and optimization: an introduction* (p. 412 pp). Boca Raton, London, New York: CRC Press, Taylor & Francis Group.
- Buttijak, W., Suchatpattamkul, K., Suksirisopha, S., & Suwansantisuk, W. (2020). Comparison of methods to tackle class imbalance in binary classification for IoT applications. In *59th annual conference of the society of instrument and control engineers of japan (sice)* (pp. 115–120). <http://dx.doi.org/10.23919/SICE48898.2020.9240403>.
- Chambers, J., Gorman, C., Feng, Y., Torn, M., & Stapp, J. (2019). Rapid remote sensing assessment of landscape-scale impacts from the California Camp fire. *PeerJ Preprint*, 7, Article e27654v1. <http://dx.doi.org/10.7287/peerj.preprints.27654v1>.
- Chong, N. S., Abdulramoni, S., Patterson, D., & Brown, H. (2019). Releases of fire-derived contaminants from polymer pipes made of polyvinyl chloride. *Toxics*, 7, Article 10. <http://dx.doi.org/10.3390/toxics7040057>.
- Devi, S., Biswas, S. K., & Purkayastha, B. (2020). A review on solution to class imbalance problem: Undersampling approaches. In *International conference on computational performance evaluation (compe)* (pp. 626–631). <http://dx.doi.org/10.1109/ComPE49325.2020.9200087>.
- Escuin, S., Navarro, R., & Fernández, P. (2008). Fire severity assessment by using NBR (normalized burn ratio) and NDVI (normalized difference vegetation index) derived from LANDSAT TM/ETM images. *International Journal of the Remote Sensing*, 29, 1053–1073. <http://dx.doi.org/10.1080/01431160701281072>.
- Farr, T. G., et al. (2007). The shuttle radar topography mission. *Review Geophysics*, 45, Article RG2004. <http://dx.doi.org/10.1029/2005RG000183>.
- Foresee, F. D., & Hagan, M. T. (1997). Gauss–Newton approximation to Bayesian regularization. In *Ieee proc. ijcn*, Vol. 1997 (pp. 1930–1935).
- Foster, D., & Mayfield, C. (2016). Geospatial resource integration in support of homeland defense and security. *IJAGR*, 7, 53–63. <http://dx.doi.org/10.4018/IJAGR.2016100105>.
- Geller, C. (2018). Automated burned area identification in real-time during wildfire events using WorldView imagery for the insurance industry. In *Proc. spie 10790 2018. earth resources and environmental remote sensing/gis applications ix*. Article 1079015. <http://dx.doi.org/10.1117/12.2324458>.
- Goss, M., Swain, D. L., Abatzoglou, J. T., Sarhadi, A., Kolden, C. A., Williams, A. P., et al. (2020). Climate change is increasing the likelihood of extreme autumn wildfire conditions across California. *Environmental Research Letters*, 15. <http://dx.doi.org/10.1088/1748-9326/ab83a7>.
- Halofsky, J. E., Peterson, D. L., & Harvey, B. J. (2020). Changing wildfire, changing forests: the effects of climate change on fire regimes and vegetation in the Pacific northwest, USA. *Fire Ecology*, 16. <http://dx.doi.org/10.1186/s42408-019-0062-8>.
- Hammer, R. B., Radeloff, V. C., Fried, J. S., & Stewart, S. I. (2007). Wildland–urban interface housing growth during the 1990s in California, Oregon, and Washington. *International Journal of the Wildland Fire*, 16, 255–265. <http://dx.doi.org/10.1071/WF05077>.
- Haro-García, A., Cerruela-García, G., & García-Pedrajas, N. (2020). Ensembles of feature selectors for dealing with class-imbalanced datasets: A proposal and comparative study. *Information Science*, 540, 89–116. <http://dx.doi.org/10.1016/j.ins.2020.05.077>.
- Haykin, S. (2009). *Neural networks and learning machines* (3rd ed.). (p. 936 pp). Upper Saddle River, New Jersey, USA: Pearson Prentice Hall.
- Hengl, T., Mendes de Jesus, J., Heuvelink, G. B. M., Ruiperez Gonzalez, M., Kilibarda, M., Blagotić, A., et al. (2017). Soilgrids250 m: Global gridded soil information based on machine learning. *PLoS One*, 12, Article e0169748. <http://dx.doi.org/10.1371/journal.pone.0169748>.
- Heris, M. P., Foks, N. L., Bagstad, K. J., Troy, A., & Ancona, Z. H. (2020). A rasterized building footprint dataset for the United States. *Science and Data*, 7, Article 10. <http://dx.doi.org/10.1038/s41597-020-0542-3>.
- Higuera, P. E., & Abatzoglou, J. T. (2020). Record-setting climate enabled the extraordinary 2020 fire season in the western United States. *Global Change Biology*, 27, 1–2. <http://dx.doi.org/10.1111/gcb.15388>.
- Holden, Z. A., Hanson, A. S., Luce, C. H., Jolly, W. M., Maneta, M., Oyler, J. W., et al. (2018). Decreasing fire season precipitation increased recent western US forest wildfire activity. *Proceedings of the National Academy of Sciences of the United States of America*, 115, 8349–8357. <http://dx.doi.org/10.1073/pnas.180231611>.
- Isaacson, K. P., Proctor, C. R., Wang, Q. E., Edwards, E. Y., Noh, Y., Shah, A. D., et al. (2021). Drinking water contamination from the thermal degradation of plastics: implications for wildfire and structure fire response. *Environmental Science: Water Research Technology*, 7, 274–284. <http://dx.doi.org/10.1039/DOWE00836B>.
- Jain, P., Coogan, S. C. P., Subramanian, S. G., Crowley, M., Taylor, S., & Flannigan, M. D. (2020). A review of machine learning applications in wildfire science and management. *Environmental Reviews*, 28, 478–505. <http://dx.doi.org/10.1139/er-2020-0019>.
- Jin, Y., Scaduto, E., & Chen, B. (2019). Fire behavior monitoring and assessment in California with multi-sensor satellite observations. *IGARSS 2019, IEEE International geoscience and remote sensing symposium*, 9972–9975. <http://dx.doi.org/10.1109/IGARSS.2019.8899094>.
- Karim, M. R., Abbaszadegan, M., & Lechavallier, M. (2003). Potential for pathogen intrusion during pressure transients. *Journal of the American Water Works Association*, 95, 134–146. <http://dx.doi.org/10.1002/j.1551-8833.2003.tb10368.x>.
- Keeley, J. E., & Syphard, A. D. (2019). Twenty-first century California, USA, wildfires: fuel-dominated vs. wind-dominated fires. *Fire Ecology*, 15. <http://dx.doi.org/10.1186/s42408-019-0041-0>.
- Knopp, L., Wieland, M., Rättich, M., & Martinis, S. (2020). A deep learning approach for burned area segmentation with sentinel-2 data. *Remote Sensing*, 12(2422), Article 12152422. <http://dx.doi.org/10.3390/rs12152422>.
- LeChevallier, M. W., Gullick, R. W., Karim, M. R., Friedman, M., & Funk, J. E. (2003). The potential for health risks from intrusion of contaminants into the distribution system from pressure transients. *Journal of the Water Health*, 1, 3–14. <http://dx.doi.org/10.2166/wh.2003.0002>.
- López, V., Fernández, A., García, S., Palade, V., & Herrera, F. (2013). An insight into classification with imbalanced data: empirical results and current trends on using data intrinsic characteristics. *Information Science*, 25, 113–141.
- MacKay, D. J. C. (1992). Bayesian interpolation. *Neural Computers*, 4, 415–447.
- Malik, A., Rao, M. R., Puppala, N., Koouri, V., Thota, V. A. K., Liu, Q., et al. (2021). Data-driven wildfire risk prediction in northern California. *Atmosphere*, 12, Article 12010109. <http://dx.doi.org/10.3390/atmos12010109>.
- Marquardt, D. (1963). An algorithm for least-squares estimation of nonlinear parameters. *SIAM Journal of the Applied Mathematics*, 11, 431–441.
- Mass, C. F., & Ovens, D. (2019). The northern California wildfires of 8–9 2017: The role of a major downslope wind event. *Bulletin American Meteorology Society*, 100, 235–256. <http://dx.doi.org/10.1175/BAMS-D-18-0037.1>.
- McWethy, D. B., Schoennagel, T., Higuera, P. E., Krawchuk, M., Harvey, B. J., Metcalf, E. C., et al. (2019). Rethinking resilience to wildfire. *Natural Sustainability*, 2, 797–804. <http://dx.doi.org/10.1038/s41893-019-0353-8>.
- Picotte, J. J., Dockter, D., Long, J., Tolk, B., Davidson, A., & Peterson, B. (2019). LANDFIRE remap prototype mapping effort: Developing a new framework for mapping vegetation classification, change, and structure. *Fire*, 2(35), Article 10. <http://dx.doi.org/10.3390/fire2020035>.
- Poggio, L., de Sousa, L. M., Batjes, N. H., Heuvelink, G. B. M., Kempen, B., Ribeiro, E., et al. (2021). Soilgrids 2.0: producing soil information for the globe with quantified spatial uncertainty. *Soil*, 7, 217–240. [http://dx.doi.org/10.5194/soil-7-\(2021\)217-2021](http://dx.doi.org/10.5194/soil-7-(2021)217-2021).
- Polikar, R. (2012). Ensemble learning. In C. Zhang, & Y. Ma (Eds.), *Ensemble machine learning*. Boston, MA: Springer. [http://dx.doi.org/10.1007/978-1-4419-9326-7\\_1](http://dx.doi.org/10.1007/978-1-4419-9326-7_1).
- Proctor, C. R., Lee, L., Yu, D., Shah, A. D., & Whelton, A. J. (2020). Wildfire caused widespread drinking water distribution network contamination. *AWWA Water Science*, Article e1183. <http://dx.doi.org/10.1002/aws.21183>.
- Proctor, C. R., Whelton, A. J., Shah, A. D., & Lee, J. (2021). Fire & water. *Civil Engineering Magazine*, 91, 42–47. <http://dx.doi.org/10.1061/ciegag.0001553>.
- Quill, R., Sharples, J. J., Wagenbrenner, N. S., Sidhu, L. A., & Forthofer, J. M. (2019). Modeling wind direction distributions using a diagnostic model in the context of probabilistic fire spread prediction. *Frontiers on Mechanical Engineering*, 5. <http://dx.doi.org/10.3389/fmech.2019.00005>.
- Radloff, V. C., Helmers, D. P., Kramer, H. A., Mockrin, M. H., Alexandre, P. M., Bar-Massada, A., et al. (2018). Rapid growth of the US wildland–urban interface raises wildfire risk. *Proceedings of the National Academy of Sciences of the United States of America*, 115, 3314–3319. <http://dx.doi.org/10.1073/pnas.1718850115>.
- Rodman, L. A., Winterkamp, J., Edminster, C., Colman, J. J., & Smith, W. S. (2017). Coupled influences of topography and wind on wildland fire behavior. *International Journal of the Wildland Fire*, 16, 183–195. <http://dx.doi.org/10.1071/WF06078>.
- Rollins, M. G. (2009). Landfire: a nationally consistent vegetation, wildland fire, and fuel assessment. *International Journal of the Wildland Fire*, 18, 235–249. <http://dx.doi.org/10.1071/WF08088>.
- Schmidt, A., Creason, W., & Law, B. E. (2018). Estimating regional effects of climate change and altered land use on biosphere carbon fluxes using distributed time delay neural networks with Bayesian regularized learning. *Neural Networks*, 108, 97–113. <http://dx.doi.org/10.1016/j.neunet.2018.08.004>.
- Schmidt, A., Mainwaring, D. B., & Maguire, D. A. (2020). Development of a tailored combination of machine learning approaches to model volumetric soil water content within a mesic forest in the Pacific Northwest. *Journal of Hydrology*, 588, Article 125044. <http://dx.doi.org/10.1016/j.jhydrol.2020.125044>.
- Schulze, S. S., & Fischer, E. C. (2021). Prediction of water distribution system contamination based on wildfire burn severity in wildland urban interface communities. *ACS ES Transactions on Water*, 1, 291–299. <http://dx.doi.org/10.1021/acs.estwater.0c00073>.
- Syphard, A. D., Rustigian-Romsos, H., Mann, V. M., Conslik, E., Moritz, M. A., & Ackerly, D. (2019). The relative influence of climate and housing development on current and projected future fire patterns and structure loss across three California landscapes. *Global Environmental Change*, 56, 41–55. <http://dx.doi.org/10.1016/j.gloenvcha.2019.03.007>.

- Tolulope, O. O., Proctor, C. R., Wang, Q. E., Sabbaghi, A., Peterson, K. S., Yu, D. J., et al. (2021). Water safety attitudes, risk perception, experiences, and education for households impacted by the 2018 camp fire. California. *Natural Hazards*, 64, <http://dx.doi.org/10.1007/s11069-021-04714-9>.
- Ullrich, P. A., Xu, Z., Rhoades, A. M., Dettinger, M. D., Mount, J. F., Jones, A. D., et al. (2018). California's drought of the future: A midcentury recreation of the exceptional conditions of 2012–2017. *Earth's Future*, 6, 1568–1587. <http://dx.doi.org/10.1029/2018EF001007>.
- Wagenbrenner, N. S., Forthofer, J. M., Lamb, B. K., Shannon, K. S., & Butler, B. W. (2016). Downscaling surface wind predictions from numerical weather prediction models in complex terrain with WindNinja. *Atmospheric Chemistry and Physics*, 16, 5229–5241. <http://dx.doi.org/10.5194/acp-16-5229-2016>.
- World Health Organization & International Programme on Chemical Safety (1996). *Health criteria and other supporting information: vol. 2, Guidelines for drinking-water quality* (2nd ed.). Accessible at: <https://apps.who.int/iris/handle/10665/38551>.
- Williams, A. P., Abatzoglou, J. T., Gershunov, A., et al. (2019). Observed impacts of anthropogenic climate change on wildfire in California. *Earth's Future*, 7, 892–910. <http://dx.doi.org/10.1029/2019EF001210>.
- Wilson, J. P., & Gallant, J. C. (Eds.), (2000). *Terrain analysis: principles and applications* (p. 520). New York: John Wiley & Sons, Inc.
- Zevenbergen, L. W., & Thorne, C. R. (1987). Quantitative analysis of land surface topography. *Earth Surface Processing and Landforms*, 12, 47–56.
- Zhang, G., Wang, M., & Liu, K. (2019). Forest fire susceptibility modeling using a convolutional neural network for yunnan province of China. *International Journal of the Disaster Risk Sciences*, 10, 386–403. <http://dx.doi.org/10.1007/s13753-019-00233-1>.
- Zulkifli, S. N., Rahim, H. A., & Lau, W. J. (2018). Detection of contaminants in water supply: A review on state-of-the-art monitoring technologies and their applications. *Sensors Actuators B: Chemicals*, 255, 2657–2689. <http://dx.doi.org/10.1016/j.snb.2017.09.078>.